Available online at www.sciencedirect.com
SCIENCE DIRECT
Journal of Structural Biology 154 (2006) 327–332
Journal of Structural Biology
www.elsevier.com/locate/yjsbi

Crystallization note

Crystal structure of human pyridoxal kinase

Peng Cao [a,1], Yong Gong [a,1], Lin Tang [a], Yun-Chung Leung [b], Tao Jiang [a,*]

[a] *National Laboratory of Biomacromolecules, Institute of Biophysics, Chinese Academy of Sciences, 15 Datun Road, Chaoyang District, Beijing 100101, China*
[b] *Department of Applied Biology and Chemical Technology, The Hong Kong Polytechnic University, Hung Hom, Kowloon, Hong Kong, China*

Received 6 January 2006; received in revised form 20 February 2006; accepted 22 February 2006
Available online 20 March 2006

Abstract

Pyridoxal kinase, a member of the ribokinase superfamily, catalyzes the ATP-dependent phosphorylation reaction of vitamin B6 and is an essential enzyme in the formation of pyridoxal-5′-phosphate, a key cofactor for over 100 enzymes. Pyridoxal kinase is thus regarded as a potential target for pharmacological agents. In this paper, we report the 2.8 Å crystal structure of human pyridoxal kinase (HPLK) expressed in *Escherichia coli*. The diffraction data revealed unexpected merohedral perfect twinning along the crystallographic *c* axis. Taking perfect twinning into account, the structure in dimeric form was well refined according to the CNS program. Structure comparison reveals that the key 12-residue peptide over the active site in HPLK is a β-strand/loop/β-strand flap, while the corresponding peptide in sheep brain enzyme adopts a loop conformation. Moreover, HPLK possesses a more hydrophobic ATP-binding pocket. This structure will facilitate further biochemical studies and structure-based design of drugs related to pyridoxal kinase.

Keywords: Human pyridoxal kinase; Crystal structure; Perfect twinning; Pyridoxal-5′-phosphate

1. Introduction

Pyridoxal-5′-phosphate (PLP)[2] is described as the most versatile organic cofactor in biology for taking part in numerous kinds of reactions in intermediary metabolism and associating with the synthesis of neurotransmitters (Shetty and Gaitonde, 1980; Ubbink et al., 1990). Mammals cannot synthesize PLP de novo and require the precursors of vitamin B6, namely pyridoxal, pyridoxamine, and pyridoxine, from diet (McCormick and Chen, 1999). Pyridoxal kinase (PLK) catalyzes the ATP-dependent phosphorylation reaction of vitamin B6 precursors and plays an essential role in the formation of biologically active form PLP (McCormick and Snell, 1961).

In the body, PLP is first synthesized by PLK in the liver, and then released to the bloodstream in association with albumin. Circulating PLP is dephosphorylated by membrane-associated phosphatases to gain entry to target cells and then converted back to PLP by intracellular PLK (Lumeng et al., 1980; Merrill et al., 1984). After the intracellular phosphorylation reaction, PLK is considered not to release PLP directly, but to interact with PLP-dependent enzymes and deliver PLP to the latter to avoid premature PLP hydrolysis (Cheung et al., 2003).

Human pyridoxal kinase (HPLK) is of particular interest because of the intimate relationship of PLP to human disorders. For broad substrate specificity (McCormick and Chen, 1999), HPLK can be inhibited by some drugs, such as theophylline and progabide, which result in vitamin B6 deficiency and various side-effects related to the central nervous system (Laine-Cessac et al., 1997). On the other hand, some drugs can stimulate the activity of PLK to induce depression synomone (Shetty and Gaitonde, 1980). Moreover, according to recent data, a supraphysiological amount of PLP exerts anti-proliferative and anti-tumoral

* Corresponding author. Fax: +86 10 64888510.
E-mail address: x-ray@sun5.ibp.ac.cn (T. Jiang).
[1] These authors contributed equally to this work.
[2] Abbreviations used: PLK, pyridoxal kinase; HPLK, human pyridoxal kinase; PLP, pyridoxal 5′-phosphate.

1047-8477/$ - see front matter © 2006 Elsevier Inc. All rights reserved.
doi:10.1016/j.jsb.2006.02.008

activities (Vermeersch et al., 2004). Therefore, HPLK is regarded as a potential target for pharmacological agents.

The three-dimensional structures of sheep brain PLK alone and in complex with substrates or products (PLK/ATP, PLK/AMP-PCP/pyridoxamine, PLK/ADP/PLP, and PLK/ADP) were solved, elucidating the conformational changes of PLK in the phosphorylation process (Li et al., 2002, 2004). Recently, the crystal structures of sheep brain PLK in complex with Roscovitine and derivatives were reported (Tang et al., 2005). Roscovitine is a promising anti-tumor drug that binds PLK at the pyridoxal-binding site. Although, the expression and purification of HPLK have been reported for several years (di Salvo et al., 2004; Hanna et al., 1997; Lee et al., 2000), the crystal structure remained unknown.

In this article, the crystal structure of HPLK at 2.8 Å resolution was reported for the first time, and structural differences between HPLK and sheep brain PLK were discussed.

2. Experimental procedures

2.1. Protein expression and purification

The HPLK recombinant plasmid was purchased from Genecopoeia Company in the name of OmicsLink™ ORF Expression Clone (EX-K1939-B01), which contained an N-terminal polyhistidine tag sequence. The plasmid was transformed into *Escherichia coli* strain BL21 (DE3) plysS (Novagen) and expressed in LB medium. The recombinant protein was purified through affinity chromatography and size-exclusion chromatography using Ni–NTA agarose and HiLoad 26/60 Superdex 200 gel-filtration column (Amersham Biosciences), respectively. The purity and homogeneity of the fractions were analyzed by SDS–PAGE. The purified HPLK was concentrated to 20 mg/ml with a Millipore spin filter (10 000 Da cut-off) in the buffer containing 50 mM Tris–HCl, pH 8.0, 150 mM NaCl, and 1 mM DTT, subsequently frozen in aliquots, and stored at −80 °C.

2.2. Crystallization and X-ray data collection

All crystallization trials were performed at 290 K using the hanging drop vapor diffusion method. Commercially available crystallization screening kits Index and SaltRx (Hampton Research, Laguna Niguel, CA) were used for initial screening, and microcrystals were obtained from several conditions. Crystals were obtained by mixing 2 μl HPLK protein solution (20 mg/ml, 50 mM Tris–HCl, pH 8.0, 150 mM NaCl, and 1 mM DTT) with 1 μl reservoir solution and against 1 ml reservoir containing 0.1 M Tris–HCl, pH 8.0, 1.80 M NH_4Ac, and 3% glycol. After incubation for about 2–3 days, crystals grew to a useful size (typically, 0.3 mm × 0.3 mm × 0.2 mm).

Before data collection, the crystal was cryoprotected by brief soaking in mother liquor containing 8% (volume/volume) 1,4-butanediol and flash-cooled in liquid nitrogen. X-ray diffraction data were collected using the Rigaku *R*-Axis-IP IV++ imaging plate area detector in the Institute of Biophysics, Chinese Academy of Sciences (Beijing, China). The data were integrated and scaled with DENZO and SCALEPACK (Otwinowski and Minor, 1997).

2.3. Structure determination and refinement

Molecular replacement was carried out with the program AMoRe from the *CCP*4 program suite (Dodson et al., 1997) using the unliganded structure of sheep brain PLK (Accession Code 1LHP) as the search model. In the model, the residues 117–129 were omitted and the distinct amino acids were mutated to alanines. The CNS program (Brünger et al., 1998) was used for detwinning the data, refining coordinates and *B*-factors, and adding water molecules finally. All model building was performed manually by the program O (Jones et al., 1991). The quality of the final structure was evaluated using PROCHECK (Laskowski et al., 1993). The Ramachandran plot showed that most residues were in the favorable region and no residues were in the disallowed region. Details of the data collection and structure refinement are given in Table 1.

Table 1
Structure determination and refinement of human pyridoxal kinase

	HPLK
Data collection statistics	
Space group	$P4_3$
Cell dimension (Å)	$a = b = 52.5$, $c = 301.0$
Resolution (Å)	2.6–100.0
Unique reflections	24 880
Completeness (%)	99.5 (99.3)
R_{merge} [a,b]	0.030 (0.306)
Mean $I/\sigma(I)$	33.1(2.4)
Detwinned data statistics	
Resolution (Å)	2.8–8.0
Completeness (%)	81.0
Refinement statistics	
R_{work} [b]	0.228
R_{free} [c]	0.271
Number of protein atoms	5120
Number of water atoms	202
Root-mean-square deviation from ideal geometry of final models	
r.m.s.d bonds (Å)	0.009
r.m.s.d angles (°)	1.9
Average *B*-factor (Å^2)	
Protein atoms	44.6
Waters	49.4

[a] $R_{merge} = \sum_{\mathbf{h}}\sum_i(|I_i(\mathbf{h}) - \langle I(\mathbf{h})\rangle|)/\sum_{\mathbf{h}}\sum_i I_i(\mathbf{h})$, where $I_i(\mathbf{h})$ is the *i*th integrated intensity of a given reflection and $\langle I(\mathbf{h})\rangle$ is the weighted mean of all measurements of $I(\mathbf{h})$.

[b] $R_{work} = \sum_{\mathbf{h}} ||F(\mathbf{h})_o| - |F(\mathbf{h})_c|| / \sum_{\mathbf{h}} |F(\mathbf{h})_o|$ for the 95% of reflection data used in refinement.

[c] $R_{free} = \sum_{\mathbf{h}} ||F(\mathbf{h})_o| - |F(\mathbf{h})_c|| / \sum_{\mathbf{h}} |F(\mathbf{h})_o|$ for the 5% of reflection data excluded from refinement.

3. Results and discussion

3.1. Structure determination

HPLK crystals grew with block shaped morphology. Based on the systematic absences, we initially determined that they belonged to space group $P4_322$ corresponding to only one monomer for each asymmetric unit. Molecular replacement calculation was performed and yielded a plausible solution. However, after multiple cycles of consequent refinements, the *R*-factor was unacceptably high. We reindexed the data in $P4_3$ but the *R*-factor remained unreasonable. Therefore, the twin-fraction determination tests were performed, including the CNS script (detect_twin.inp, Brünger et al., 1998) and the twinning server (http://www.doe-mbi.ucla.edu/services/Twinning/; Yeates, 1997), and the results showed that the HPLK crystal was perfectly twinned with a twinning factor of 0.47.

After molecular replacement in $P4_3$, the data were detwinned with the twinning operator (h, −k, −l) during the detwinning procedure (CNS script detwin_perfect.inp; Schuermann et al., 2005). The electron density map was calculated with the detwinned data and the model was built according to the map. Initial simulated annealing decreased the *R*-factor to 27.5%. The subsequent procedures included iterative rounds of model building, detwinning the original diffraction data, and refinement using the detwinned data. In the final round of the detwinning step, a model with an *R*-factor of 22.8% and an *R*-free of 27.1% was obtained. The model mostly fits well with the corresponding electron density.

According to the calculated F_o-F_c electron density map, in which the polyhistidine tag was clearly displayed, the N-terminal residues of HPLK were traced. The final model refined at 2.8 Å resolution contains all residues from Met-1 to Leu-312 of HPLK and the 11 residues from the vector at the N-terminus including the polyhistidine tag. In addition, the last four residues from the vector were disordered in both monomers and were not constructed.

3.2. Overall structure

HPLK is a homodimer related by a non-crystallographic twofold axis in an asymmetric unit (Fig. 1A). Interestingly, the packing of the molecules shows that the non-crystallographic twofold axis parallels to the axis [1 1 0], which could be the reason for the perfect twinning and a pseudo laue symmetry (space group: $P4_322$). Each HPLK monomer contains nine α-helices (named α1–9), and 12 β-strands (named β1–10 and β5a, β5b). A topological diagram is shown in Fig. 1B. The 1–10 β-strands constitute a central contorted β-sheet flanked by α2, α3, α4, α5, and α6 on one side and α1, α7, α8, and α9 on the other side. The N-terminal polyhistidine tag forms an almost α-helix morphology.

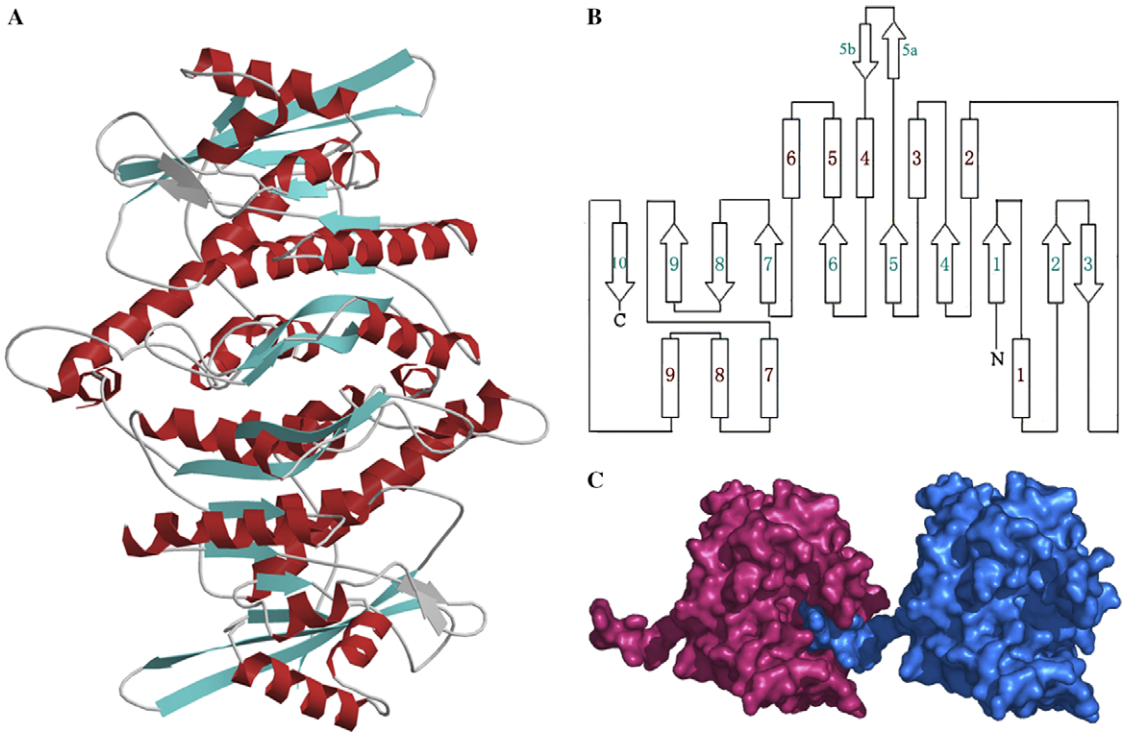

Fig. 1. Overall structure of human pyridoxal kinase. (A) A ribbon diagram representing the dimeric structure of human pyridoxal kinase viewed along the twofold axis in red for α-helices, green for β-strands, and gray for two extra β-strands absent from sheep brain pyridoxal kinase. This figure and all following figures were generated using MolScript (Kraulis, 1991), Raster3D (Merrit and Murphy, 1994), Molmol (Koradi et al., 1996), or ESPript (Gouet et al., 1999). (B) Topological diagram. α-helices are shown as rectangles and β-strands are shown as arrows. Each secondary structure element is labeled in the center (α-helices, red; β-strands, green). (C) The surfaces of two human pyridoxal kinase molecules in contact with each other through the N-terminus, which stretches out from one molecule and sticks into the other enzyme molecule.

The overall folding pattern is an αβα three-layer sandwich which is commonly shared in the ribokinase superfamily (Zhang et al., 2004). In contrast to native sheep brain PLK, there are two extra β-strands, namely β5a and β5b, inserted between β5 and α4 in HPLK. In addition, a large negative potential region is found at one side of the surface, through which HPLK might interact with PLP-dependent enzymes.

3.3. Association of molecules

HPLK is an elongated dimer with the approximate dimensions of 85 Å × 60 Å × 40 Å. The dimer interface is formed between α1, α9, β1, and β3 from each monomer with a non-crystallographic twofold symmetry through hydrogen bonding, salt bridges, and hydrophobic interactions. The buried area is approximately 1930 $Å^2$ and about 13.6% of the total surface area in one monomer. The residues Val-15, Val-35, Val-74, and Ala-287 at the dimer interface in sheep brain PLK are substituted, respectively, by more hydrophobic residues Ile-15, Ile-35, Met-74, and Met-287 in HPLK, indicating a stronger hydrophobic interaction between monomers of HPLK.

The polyhistidine tag at the N-terminus stretches out from one HPLK molecule and inserts into another, which belongs to an adjacent asymmetric unit (Fig. 1C). Therefore, the molecules in the crystal form polymers in layers. Moreover, the pyridoxal-binding site is partially occupied by the polyhistidine tag, which would be the reason why our repeated attempts to soak or cocrystallize HPLK with substrates or analogs were failed.

3.4. HPLK active site

The active sites have high structural similarity among members of the ribokinase superfamily (Zhang et al., 2004). Therefore, the location and mode of substrate binding in HPLK could be deduced by analogy to the structures of sheep brain PLK in complex with substrates (Li et al., 2002, 2004). On each enzyme surface, there is a cavity with negative charge located along one edge of the central β-sheet and this high negative potential is favorable to attract substrates with positive charge, such as the pyridine ring of vitamin B6 and the adenine ring of ATP, to bind here. A comparison of the electrostatic potential surfaces of HPLK and sheep brain PLK is shown in Figs. 2A and B.

The ATP-binding site is positioned in a shallow groove formed by the hydrophobic side chains of surrounding residues. Previous studies showed that the K_m values of ATP were 12 and 20 μM for HPLK and sheep brain PLK, respectively (Kerry and Kwok, 1986; Kerry et al., 1986). Structure comparison reveals that three residues Ala-201, Met-223, and Met-263, which interact with the adenine ring of ATP in sheep brain PLK through hydrophobic interactions, are substituted, respectively, in HPLK by more hydrophobic amino acids Val-201, Ile-223, and Leu-263. It is consistent with the biochemical result that HPLK possesses more affinity with ATP than sheep enzyme. In addition, Asn-121, which has positive potential over the ATP-binding site in sheep brain PLK, was replaced by negative potential residue Asp-121 in HPLK.

The pyridoxal-binding site is located in a pocket in the opposite direction of ATP. The residues that interact with pyridoxal through hydrogen bonds and hydrophobic interactions are highly conserved between HPLK and sheep brain PLK, including Ser-12, Thr-47, and Asp-235, etc.

3.5. Comparison between HPLK and sheep brain PLK

The superposition of HPLK and sheep brain PLK structures reveals that their main chain conformations are mostly identical except for differences in the flexible loops. The main differences are found in the loops between β5 and α4, β7 and β8, β8 and β9, and α8 and α9. A superposed illustration is shown in Fig. 2C.

According to biochemical study, HPLK is more stable than sheep brain PLK against denaturation by guanidine hydrochloride (Lee et al., 2000). It might be due to the stronger hydrophobic interactions in HPLK than sheep brain PLK.

Moreover, previous structural analysis of sheep brain PLK complexes reveals that there is a key 12-residue loop (Gly-117 to Val-128) over the active site playing an important role in the catalytic process. After ATP binding, the loop covers partially the ATP-binding site to prevent unproductive hydrolysis of ATP; when substrates are absent, the loop exhibits a different conformation and occupies neither the ATP-binding site nor the pyridoxal-binding site (Li et al., 2002, 2004; Tang et al., 2005). However, the conformation of the corresponding segment in HPLK is not a loop, but a β-strand/loop/β-strand flap. It is also noteworthy that the residue Arg-120 in the loop of sheep brain PLK is replaced by Trp-120 in HPLK, which is completely exposed to the solvent region. A multiple sequence alignment of PLKs from different special species (Fig. 2D) indicates that the key peptides (Gly-117 to Val-128 in HPLK) in advanced species consist of 12 residues, differing from

Fig. 2. Comparison between human pyridoxal kinase and sheep brain pyridoxal kinase. (A and B) Electrostatic potential surfaces of human pyridoxal kinase (A) and sheep brain pyridoxal kinase (B). Positive potential regions are blue, and negative potential regions are red. Residues-121 at the surfaces are indicated by yellow circles. ATP and pyridoxal are shown in ball-and-stick representation in (B) (ATP, green; pyridoxal, yellow). (C) Superposition of human pyridoxal kinase (purple) and sheep brain pyridoxal kinase (green). Their main chain conformations are mostly identical except in their flexible loops. (D) Sequence alignment and comparison of pyridoxal kinases from different species. From the top to bottom: human (HPLK), sheep brain, pig, *Haemophilus influenzae*, *E. coli*, and *Salmonella typhimurium*. The secondary structure elements of human pyridoxal kinase are shown above the alignment in blue. Arrows indicate β-strands and coils indicate helices. Strictly conserved and conservatively substituted residues are boxed and marked with red and yellow background, respectively. Conserved residues between human and sheep brain are indicated by red letters. The key 12-residue peptide is marked by green triangles. The conserved glycine–glycine dipeptide region is marked by purple stars and the last conserved residue Asp is in purple.

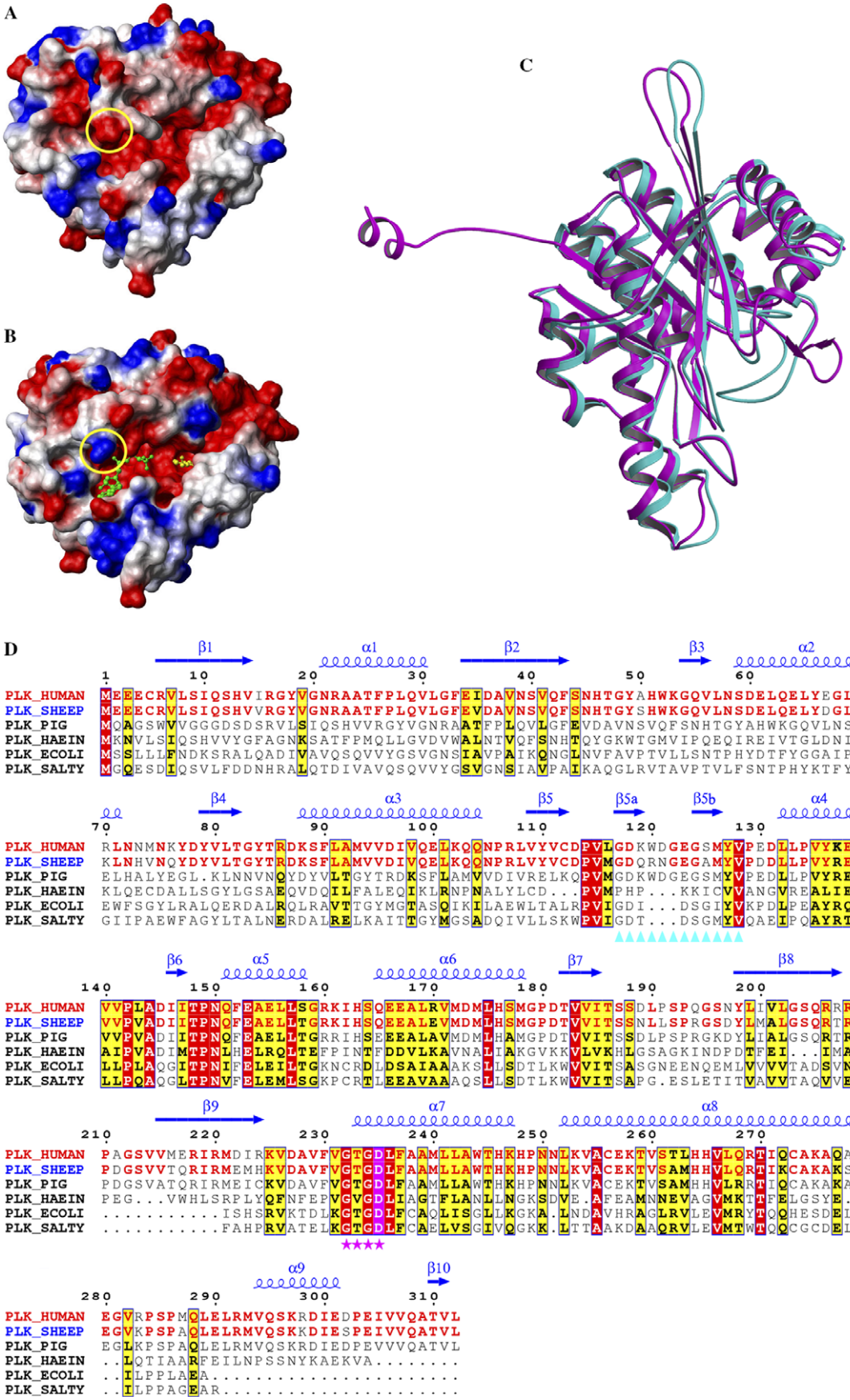
A
B
C
D
β1 α1 β2 β3 α2
1 10 20 30 40 50 60
PLK_HUMAN MEEECRVLSIQSHVIRGYVGNRAATFPLQVLGFEIDAVNSVQFSNHTGYAHWKGQVLNSDELQELYEGL.
PLK_SHEEP MEEECRVLSIQSHVVRGYVGNRAATFPLQVLGFEVDAVNSVQFSNHTGYSHWKGQVLNSDELQELYDGL.
PLK_PIG MQAGSWVVGGGDSDSRVLSIQSHVVRGYVGNRAATFPLQVLGFEVDAVNSVQFSNHTGYAHWKGQVLNSD
PLK_HAEIN MKNVLSIQSHVVYGFAGNKSATFPMQLLGVDVWALNTVQFSNHTQYGKWTGMVIPQEQIREIVTGLDNIE
PLK_ECOLI MSSLLLFNDKSRALQADIVAVQSQVVYGSVGNSIAVPAIKQNGLNVFAVPTVLLSNTPHYDTFYGGAIPD
PLK_SALTY MGQESDIQSVLFDDNHRALQTDIVAVQSQVVYGSVGNSIAVPAIKAQGLRVTAVPTVLFSNTPHYKTFYG
β4 α3 β5 β5a β5b α4
70 80 90 100 110 120 130
PLK_HUMAN RLNNMNKYDYVLTGYTRDKSFLAMVVDIVQELKQQNPRLVYVCDPVLGDKWDGEGSMYVPEDLLPVYKEK
PLK_SHEEP KLNHVNQYDYVLTGYTRDKSFLAMVVDIVQELKQQNPRLVYVCDPVMGDQRNGEGAMYVPDDLLPVYREK
PLK_PIG ELHALYEGL.KLNNVNQYDYVLTGYTRDKSFLAMVVDIVRELKQPVMGDKWDGEGSMYVPEDLLPVYREK
PLK_HAEIN KLQECDALLSGYLGSAEQVDQILFALEQIKLRNPNALYLCD...PVMPHP...KKICVVANGVREALIEK
PLK_ECOLI EWFSGYLRALQERDALRQLRAVTTGYMGTASQIKILAEWLTALRPVIGDI...DSGIYVKPDLPEAYRQY
PLK_SALTY GIIPAEWFAGYLTALNERDALRELKAITTGYMGSADQIVLLSKWPVIGDT...DSGMYVQAEIPQAYRTH
β6 α5 α6 β7 β8
140 150 160 170 180 190 200
PLK_HUMAN VVPLADIITPNQFEAELLSGRKIHSQEEALRVMDMLHSMGPDTVVITSSDLPSPQGSNYLIVLGSQRRRN
PLK_SHEEP VVPVADIITPNQFEAELLTGRKIHSQEEALEVMDMLHSMGPDTVVITSSNLLSPRGSDYIMALGSQRTRA
PLK_PIG VVPVADIITPNQFEAELLTGRRIHSEEEALAVMDMLHAMGPDTVVITSSDLPSPRGKDYLIALGSQRTRS
PLK_HAEIN AIPVADIMTPNLHELRQLTEFPINTFDDVLKAVNALIAKGVKKVLVKHLGSAGKINDPDTFEI...IMAT
PLK_ECOLI LLPLAQGITPNIFELEILTGKNCRDLDSAIAAAKSLLSDTLKWVVITSASGNEENQEMLVVVTADSVNV
PLK_SALTY LLPQAQGLTPNVFELEMLSGKPCRTLEEAVAAAQSLLSDTLKWVVITSAPG.ESLETITVAVVTAQVVEV
β9 α7 α8
210 220 230 240 250 260 270
PLK_HUMAN PAGSVVMERIRMDIRKVDAVFVGTGDLFAAMLLAWTHKHPNNLKVACEKTVSTLHHVLQRTIQCAKAQAG
PLK_SHEEP PDGSVVTQRIRMEMHKVDAVFVGTGDLFAAMLLAWTHKHPNNLKVACEKTVSAMHHVLQRTIKCAKAKSG
PLK_PIG PDGSVATQRIRMEICKVDAVFVGTGDLFAAMLLAWTHKHPNNLKVACEKTVSAMHHVLRRTIQCAKAKAG
PLK_HAEIN PEG...VWHLSRPLYQFNFEPVGVGDLIAGTFLANLLLNGKSSDVE.AFEAMNNEVAGVMKTTFELGSYE..
PLK_ECOLI ..........ISHSRVKTDLKGTGDLFCAQLISGLLKGKKA.LNDAVHRAGLRVLEVMRVTQQHESDEL.
PLK_SALTY ..........FAHPRVATELKGTGDLFCAELVSGIVQGKK.LTTAAKDAAQRVLEVMTWTQQCGCDEL.
α9 β10
280 290 300 310
PLK_HUMAN EGVRPSPMQLELRMVQSKRDIEDPEIVVQATVL
PLK_SHEEP EGVKPSPAQLELRMVQSKKDIESPEIVVQATVL
PLK_PIG EGLKPSPAQLELRMVQSKRDIEDPEVVVQATVL
PLK_HAEIN ..LQTIAARFEILNPSSNYKAEKVA.....
PLK_ECOLI ..ILPPLAEA.....
PLK_SALTY ..ILPPAGEAR.....

nine residues in lower species. The differences between the conformations of the peptides of HPLK and sheep brain PLK suggest that not only the length and the sequence (Li et al., 2002, 2004), but also the conformation of the peptide might serve as an indicator of change along the evolutionary pathway of the PLK family from simple to complex.

In conclusion, we have presented the crystal structure of HPLK for the first time. Structure comparison reveals some different structural characteristics between HPLK and sheep brain PLK. The design and modification of the drugs related to HPLK will be facilitated by the three-dimensional structure of HPLK and further studies on its complexes.

3.6. Accession number

The atomic coordinates and structure factors have been deposited in the RCSB Protein Data Bank under Accession Code 2F7K.

Acknowledgments

This project was supported by Grants from the National Key Basic Research Program (2004CB520801 and 2004CB720000), the National Natural Science Foundation of China (10490193), and the National High Technology Research and Development Program of China (2002BA411A13).

References

Brünger, A.T., Adams, P.D., Clore, G.M., DeLano, W.L., Gros, P., Grosse-Kunstleve, R.W., Jiang, J.S., Kuszewski, J., Nilges, M., Pannu, N.S., Read, R.J., Rice, L.M., Simonson, T., Warren, G.L., 1998. Crystallography & NMR system: a new software suite for macromolecular structure determination. Acta Crystallogr. D 54, 905–921.

Cheung, P.Y., Fong, C.C., Ng, K.T., Lam, W.C., Leung, Y.C., Tsang, C.W., Yang, M., Wong, M.S., 2003. Interaction between pyridoxal kinase and pyridoxal-5-phosphate-dependent enzymes. J. Biochem. 134, 731–738.

di Salvo, M.L., Hunt, S., Schirch, V., 2004. Expression, purification, and kinetic constants for human and *Escherichia coli* pyridoxal kinases. Protein Expr. Purif. 36, 300–306.

Dodson, E.J., Winn, M., Ralph, A., 1997. Collaborative computational project, number 4: providing programs for protein crystallography. Methods Enzymol. 277, 620–633.

Gouet, P., Courcelle, E., Stuart, D.I., Metoz, F., 1999. ESPript: analysis of multiple sequence alignments in PostScript. Bioinformatics 15, 305–308.

Hanna, M.C., Turner, A.J., Kirkness, E.F., 1997. Human pyridoxal kinase. cDNA cloning, expression, and modulation by ligands of the benzodiazepine receptor. J. Biol. Chem. 272, 10756–10760.

Jones, J.A., Zou, J.Y., Cowan, S.W., Kjeldgaard, M., 1991. Improved methods for building protein models in electron density maps and the location of errors in these models. Acta Crystallogr. A 47, 110–119.

Kerry, J.A., Kwok, F., 1986. Purification and characterization of pyridoxal kinase from human erythrocytes. Prep. Biochem. 16, 199–216.

Kerry, J.A., Rohde, M., Kwok, F., 1986. Brain pyridoxal kinase. Purification and characterization. Eur. J. Biochem. 158, 581–585.

Koradi, R., Billeter, M., Wüthrich, K., 1996. MOLMOL: a program for display and analysis of macromolecular structures. J. Mol. Graph. 14 (51–5), 29–32.

Kraulis, P.J., 1991. MOLSCRIPT: a program to produce both detailed and schematic plots of protein structures. J. Appl. Crystallogr. 24, 946–950.

Laine-Cessac, P., Cailleux, A., Allain, P., 1997. Mechanisms of the inhibition of human erythrocyte pyridoxal kinase by drugs. Biochem. Pharmacol. 54, 863–870.

Laskowski, R.A., MacArthur, M.W., Moss, D.S., Thornton, J.M., 1993. PROCHECK: a program to check the stereochemical quality of protein structures. Appl. Crystallogr. 26, 283–291.

Lee, H.S., Moon, B.J., Choi, S.Y., Kwon, O.S., 2000. Human pyridoxal kinase: overexpression and properties of the recombinant enzyme. Mol. Cells 10, 452–459.

Li, M.H., Kwok, F., Chang, W.R., Lau, C.K., Zhang, J.P., Lo, S.C., Jiang, T., Liang, D.C., 2002. Crystal structure of brain pyridoxal kinase, a novel member of the ribokinase superfamily. J. Biol. Chem. 277, 46385–46390.

Li, M.H., Kwok, F., Chang, W.R., Liu, S.Q., Lo, S.C., Zhang, J.P., Jiang, T., Liang, D.C., 2004. Conformational changes in the reaction of pyridoxal kinase. J. Biol. Chem. 279, 17459–17465.

Lumeng, L., Lui, A., Li, T.K., 1980. Plasma content of B6 vitamins and its relationship to hepatic vitamin B6 metabolism. J. Clin. Invest. 66, 688–695.

McCormick, D.B., Chen, H., 1999. Update on interconversions of vitamin B-6 with its coenzyme. J. Nutr. 129, 325–327.

McCormick, D.B., Snell, E.E., 1961. Pyridoxal phosphokinases. II. Effects of inhibitors. J. Biol. Chem. 263, 2085–2088.

Merrill, A.H., Henderson, J.M., Wang, E., McDonald, B.W., Millikan, W.J., 1984. Metabolism of vitamin B-6 by human liver. J. Nutr. 114, 1664–1674.

Merrit, E.A., Murphy, M.E.P., 1994. Raster3D Version 2.0. A program for photorealistic molecular graphics. Acta Crystallogr. D 50, 869–873.

Otwinowski, Z., Minor, W., 1997. Processing of X-ray diffraction data collected in oscillation mode. Methods Enzymol. 276, 307–326.

Schuermann, J.P., Prewitt, S.P., Davies, C., Deutscher, S.L., Tanner, J.J., 2005. Evidence for structural plasticity of heavy chain complementarity-determining region 3 in antibody-ssDNA recognition. J. Mol. Biol. 347, 965–978.

Shetty, K.T., Gaitonde, B.B., 1980. Effect of contraceptive steroids on gamma-aminobutyric acid metabolism and pyridoxal kinase activity in rat brain. Exp. Neurol. 70, 146–154.

Tang, L., Li, M.H., Cao, P., Wang, F., Chang, W.R., Bach, S., Reinhardt, J., Ferandin, Y., Galons, H., Wan, Y., Gray, N., Meijer, L., Jiang, T., Liang, D.C., 2005. Crystal structure of pyridoxal kinase in complex with roscovitine and derivatives. J. Biol. Chem. 280, 31220–31229.

Ubbink, J.B., Vermaak, W.J., Delport, R., Serfontein, W.J., Bartel, P., 1990. The relationship between vitamin B6 metabolism, asthma, and theophylline therapy. Ann. NY Acad. Sci. 585, 285–294.

Vermeersch, J.J., Christmann-Franck, S., Karabashyan, L.V., Fermandjian, S., Mirambeau, G., Der Garabedian, P.A., 2004. Pyridoxal 5′-phosphate inactivates DNA topoisomerase IB by modifying the lysine general acid. Nucleic Acids Res. 32, 5649–5657.

Yeates, T.O., 1997. Detecting and overcoming crystal twinning. Methods Enzymol. 276, 344–358.

Zhang, Y., Dougherty, M., Downs, D.M., Ealick, S.E., 2004. Crystal structure of an aminoimidazole riboside kinase from *Salmonella enterica*: implications for the evolution of the ribokinase superfamily. Structure 12, 1809–1821.